Rescue from excitotoxicity and axonal degeneration accompanied by age-dependent behavioral and neuroanatomical alterations in caspase-6-deficient mice

Valeria Uribe[1,†], Bibiana K.Y. Wong[1,†], Rona K. Graham[1], Corey L. Cusack[2], Niels H. Skotte[1,3], Mahmoud A. Pouladi[1], Yuanyun Xie[1], Konstantin Feinberg[4], Yimiao Ou[4], Yingbin Ouyang[8], Yu Deng[1], Sonia Franciosi[1], Nagat Bissada[1], Amanda Spreeuw[1], Weining Zhang[1], Dagmar E. Ehrnhoefer[1], Kuljeet Vaid[1], Freda D. Miller[4,5,6], Mohanish Deshmukh[2], David Howland[7] and Michael R. Hayden[1,*]

[1]Department of Medical Genetics, Centre for Molecular Medicine and Therapeutics, Child and Family Research Institute, University of British Columbia, Vancouver, British Columbia V5Z 4H4, Canada, [2]Department of Cell and Developmental Biology and Neuroscience Center, University of North Carolina, Chapel Hill, NC 27599-7250, USA, [3]Department of Medical Genetics, Institute of Cellular and Molecular Medicine, University of Copenhagen, 2200 N Copenhagen, Denmark, [4]Developmental and Stem Cell Biology Group, Hospital for Sick Children, Toronto, Ontario M5G1L7, Canada, [5]Department of Molecular Genetics and [6]Department of Physiology, University of Toronto, Toronto, Ontario M5G1X5, Canada, [7]CHDI Foundation, Inc., New York, NY 10001, USA and [8]Taconic Biosciences, Cranbury, NJ 08512, USA

Apoptosis, or programmed cell death, is a cellular pathway involved in normal cell turnover, developmental tissue remodeling, embryonic development, cellular homeostasis maintenance and chemical-induced cell death. Caspases are a family of intracellular proteases that play a key role in apoptosis. Aberrant activation of caspases has been implicated in human diseases. In particular, numerous findings implicate Caspase-6 (Casp6) in neurodegenerative diseases, including Alzheimer disease (AD) and Huntington disease (HD), highlighting the need for a deeper understanding of Casp6 biology and its role in brain development. The use of targeted caspase-deficient mice has been instrumental for studying the involvement of caspases in apoptosis. The goal of this study was to perform an in-depth neuroanatomical and behavioral characterization of constitutive Casp6-deficient (Casp6−/−) mice in order to understand the physiological function of Casp6 in brain development, structure and function. We demonstrate that Casp6−/− neurons are protected against excitotoxicity, nerve growth factor deprivation and myelin-induced axonal degeneration. Furthermore, Casp6-deficient mice show an age-dependent increase in cortical and striatal volume. In addition, these mice show a hypoactive phenotype and display learning deficits. The age-dependent behavioral and region-specific neuroanatomical changes observed in the Casp6−/− mice suggest that Casp6 deficiency has a more pronounced effect in brain regions that are involved in neurodegenerative diseases, such as the striatum in HD and the cortex in AD.

*To whom correspondence should be addressed. Tel: +1 6048753535; Fax: +1 6048753819; Email: mrh@cmmt.ubc.ca
†The authors wish it to be known that, in their opinion, the first two authors should be regarded as joint First Authors.

INTRODUCTION

Apoptosis, or programmed cell death, is a highly regulated process involved in embryonic development, developmental tissue remodeling and normal cell turnover (1,2). However, when dysregulation occurs in apoptotic pathways, excessive or insufficient cell death can lead to diseases such as cancers, autoimmune syndromes and/or neurodegenerative diseases (3,4). Caspases are a family of intracellular cysteine-aspartic proteases that are not only essential for triggering programmed cell death (5,6), but have also been shown to play key roles in non-apoptotic pathways, such as differentiation and proliferation of diverse cell types, axon guidance and synaptic activity and plasticity (7–11).

Caspases are divided into long prodomain caspases (caspases-2, -8, -9 and -10), which are initiators of apoptosis, and short prodomain caspases (caspases-3, -6, -7 and -14), which are generally termed the effectors of apoptosis (12). However, some caspases, including caspase-3 (Casp3) and caspase-6 (Casp6), appear to function as both initiators and effectors. For example, active Casp6 is observed in preclinical Alzheimer disease (AD) and Huntington disease (HD) brains years prior to overt cell death and can activate caspases-2, -3 and -8 (13–16). Similarly, activation of Casp3 has been detected concomitantly with memory loss in a murine model of AD and before obvious detection of cell death (17). Casp3 has also been shown to activate Casp6 in certain experimental paradigms (16).

Aberrant activation of caspases has been implicated in several neurodegenerative diseases, such as AD, HD, various ataxias and amyotrophic lateral sclerosis (13,18–22). Recently, Casp6 has also been implicated in ischemic brain injury (23). In mouse models of AD, baseline Casp3 activity has been shown to be elevated in hippocampal dendritic spines (17). Interestingly, inhibiting caspase cleavage of β-amyloid precursor protein (APP) at aa664, a described Casp6 cleavage site, results in the rescue of AD-like behavioral and neuropathological phenotypes (18,24–30). Furthermore, cleaved APP binds to the death receptor 6 (DR6), which activates Casp6, resulting in axonal degeneration in an AD mouse model (31).

Casp6 cleavage of mutant huntingtin (mhtt) at amino acid 586 has also been shown to be a rate-limiting step in the pathogenesis of HD (32,33). Mice carrying mhtt resistant to cleavage by Casp6 maintain normal neuronal function, do not develop striatal neurodegeneration and are protected against neurotoxicity (14,32,34–36). Recently, Casp6 activity levels in the brain were also shown to be positively correlated with CAG size and to be increased in persons carrying the mutation but being asymptomatic (14).

Given the various findings implicating Casp6 in the progression of neurodegenerative diseases and the efforts underway to identify Casp6 inhibitors as a therapeutic strategy for neurological diseases (37,38), understanding the normal role of Casp6 in brain development and structure is crucial. Therefore, the goal of this study was to perform an in-depth neuropathological and behavioral characterization of mice lacking in Casp6 (*Casp6*−/−).

We demonstrate that *Casp6*−/− neurons are protected against both nerve growth factor (NGF)-deprivation-induced axonal degeneration and neurotoxic stimulus *N*-methyl-D-aspartic acid (NMDA)-mediated excitotoxicity, thereby strengthening the evidence for a crucial role for Casp6 in this process. Similar to axons lacking p75 neurotrophin receptor (p75NTR) (39), *Casp6*−/− axons were also observed in the white matter tract of the corpus callosum, which is uncommon in normal axons. These findings validate the role of Casp6 in myelin-dependent axon degeneration in the brain.

We show that Casp6-deficient mice show an age-dependent increase in cortical and striatal volume. In addition, they show a hypoactive phenotype and display a learning deficit. The age-dependent behavioral and neuroanatomical changes observed in the *Casp6*−/− mice suggest that Casp6 deficiency has a more pronounced effect in brain regions including the striatum and cortex that are initially affected in HD and AD, respectively.

RESULTS

Casp6−/− brain and peripheral tissues show no Casp6 expression

Exons 2–5 of the *Casp6* gene encode the catalytic domain of the Casp6 protein (40). These exons were removed to generate *Casp6* knockout (*Casp6*−/−) mice that express a truncated and inactive form of Casp6 (Supplementary Material, Fig. S1A and B). Two PCR assays were designed for genotyping: the wild-type (WT) assay amplifies the WT allele from *Casp6* WT and heterozygous (*Casp6*+/−) mice; and the neo assay amplifies the knocked out allele from *Casp6*+/− and *Casp6*−/− mice. DNA extracted from *Casp6*−/− mice shows PCR products generated with the neo primers. In contrast, no PCR products are detected in *Casp6*−/− DNA, using the WT primers (Supplementary Material, Fig. S1C).

These mice were then examined by quantitative reverse transcriptase PCR (qRT-PCR) and western analysis to confirm the absence of *Casp6* expression and Casp6 protein in brain and peripheral tissues of *Casp6*−/− mice. Quantitative RT-PCR shows no *Casp6* mRNA expression in *Casp6*−/− and reduced *Casp6* mRNA expression in *Casp6*+/− brain tissue (Fig. 1A; ANOVA $P = 0.0001$). Western blotting using a Casp6 antibody demonstrates the absence of the Casp6 protein in *Casp6*−/− cerebellum, hippocampus, striatum, cortex, kidney, liver, spleen and post-natal day 0 (P0) peripheral tissue (Fig. 1B). These findings confirm that the *Casp6*−/− mice used in this study constitutively lack Casp6.

Casp6−/− sympathetic neurons show protection against axonal degeneration

Axonal degeneration is a crucial process for normal neurodevelopment (41,42) and is disturbed in neurological disorders (31,43,44). It has recently been established that axonal degeneration in both an AD mouse model and after growth factor deprivation at axon terminals is mediated through the activation of Casp6 (31,39).
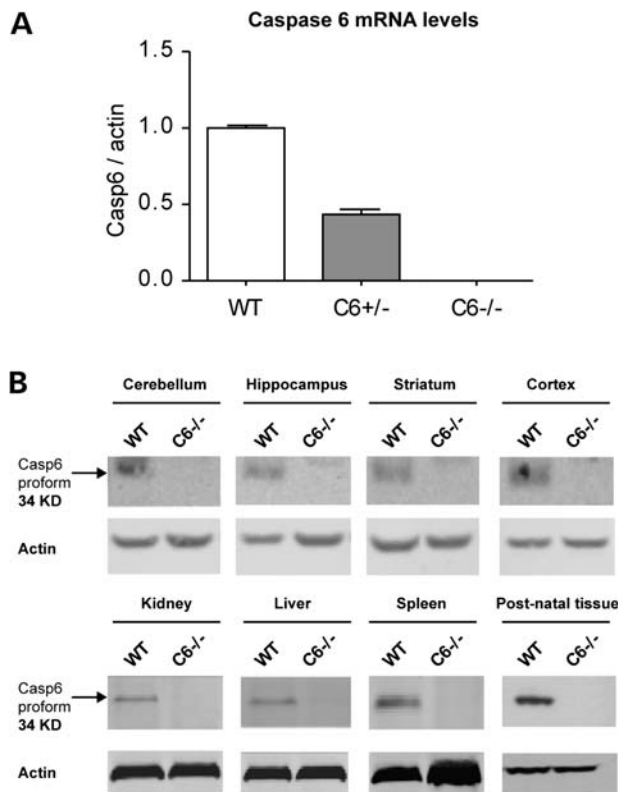
Figure 1. No Casp6 expression is observed in *Casp6−/−* brain and peripheral tissues. (**A**) Quantitative RT-PCR shows the absence of Casp6 mRNA expression in *Casp6−/−* brain tissue and reduced expression in *Casp6+/−* brain tissue when compared with WT ($n = 3$–4/genotype). (**B**) Western blots using Casp6 antibody show the absence of Casp6 protein in *Casp6−/−* cerebellum, hippocampus, striatum, cortex, kidney, liver, spleen and post-natal P0 peripheral tissue ($n = 3$/genotype).

Enhanced axonal degeneration may also explain the early white matter loss that is seen in individuals with HD and AD (45–47).

We investigated whether *Casp6−/−* sympathetic neurons are protected from axonal degeneration after NGF withdrawal. Sympathetic neurons were cultured in microfluidic chambers to allow deprivation of NGF from the axon compartment. Although axons of WT sympathetic neurons degenerate after NGF deprivation (Fig. 2A and C; *t*-test $P < 0.0001$), NGF withdrawal did not induce axonal degeneration in *Casp6−/−* sympathetic neurons (Fig. 2B and C; *t*-test $P = 0.24$) ($n = 3$ chambers/condition/genotype).

Medium spiny neurons from *Casp6+/−* and *Casp6−/−* mice show protection against NMDA-mediated excitotoxicity in a Casp6-dose-dependent manner

Casp6 inhibitors and/or dominant-negative inhibition of Casp6 provide protection against excitotoxic stress (14,15). Therefore, we hypothesized that medium spiny neurons (MSNs) derived from *Casp6*-deficient mice might be protected from NMDAR-mediated excitotoxicity. *Casp6−/−* MSNs demonstrate a significant decrease in LDH levels (Fig. 3A; one-way ANOVA $P = 0.01$, *post hoc* Tukey WT versus *Casp6−/−* $P < 0.05$,

$n = 10$ cultures), a significant increase in levels of ATP (Fig. 3B; one-way ANOVA $P = 0.03$, *post hoc* Tukey WT versus *Casp6−/−* $P < 0.05$, $n = 10$ cultures) and reduced TUNEL-positive cells (Fig. 3C and Supplementary Material S2; one-way ANOVA $P = 0.02$, *post hoc* Tukey WT versus *Casp6−/−* and WT versus *Casp6+/−* $P < 0.05$, $n = 9$–12 cultures) compared with WT MSNs post-NMDA treatment, indicative of protection against NMDAR-mediated excitotoxicity in *Casp6−/−* MSNs. Furthermore, *post hoc* linear trend test reveals a dose-dependent effect, where the *Casp6+/−* mice also demonstrate partial rescue from NMDAR-mediated excitotoxicity (*post hoc* test for linear trend, LDH: $P = 0.005$; ATP: $P = 0.01$; TUNEL: $P = 0.02$).

Casp6 is necessary for myelin-induced degeneration of septal cholinergic axons *in vivo*

A recent study demonstrated that axon degeneration was an ongoing process in the mature adult brain and implicated a p75NTR-mediated pathway in this process. Immunostaining of choline acetyltransferase (ChAT) allowed visualization of cholinergic axons that projected from the forebrain to the hippocampus by way of the supracallosal pathway, which is immediately adjacent to the corpus callosum.

In WT mice, any axons of septal cholinergic neurons that sprouted on to the myelinated corpus callosum degenerated, whereas axons in p75NTR-null mice grew and survived on this myelin tract (39). Since p75NTR-mediated axon degeneration requires Casp6 *in vitro* (39), we determined whether genetic ablation of Casp6 inhibited axonal degeneration *in vivo*.

Axon number and length were measured in 3- and 8-month-old mice. In *Casp6+/−* mice, only a few short ChAT-positive axons were observed on the white matter of the corpus callosum (Fig. 4A), which is consistent with WT littermate controls and previous WT data from the previous study (39) (data not shown). Therefore, WT and *Casp6+/−* data were combined as one control group. In contrast, in brains of *Casp6−/−* mice, more ChAT-positive axons were evident in the corpus callosum and many of these were very long (Fig. 4A).

Quantification of these results verified that at 3 and 8 months of age, more ChAT-positive axons grew on the corpus callosum in *Casp6−/−* versus control mice (Fig. 4B; two-way ANOVA genotype: $P = 0.037$, age: $P < 0.0001$, interaction: $P = 0.76$, $n = 3$–4 controls, 3–4 *Casp6−/−*), and that the total length of these axons was significantly increased (Fig. 4C; two-way ANOVA genotype: $P = 0.0015$, age: $P < 0.0001$, interaction: $P = 0.88$, $n = 3$–4 control, 3–4 *Casp6−/−*). Even after normalizing for the increased number of axons growing on the corpus callosum, axons in *Casp6−/−* mice were significantly longer than those in control mice at both ages (Fig. 4D; two-way ANOVA genotype: $P = 0.037$, age: $P = 0.86$, interaction: $P = 0.96$, $n = 3$–4 control, 3–4 *Casp6−/−*). Moreover, although many ChAT-positive axons grew continuously over the white matter in *Casp6−/−* brains, axons growing in the control brains appeared to be degenerating (Fig. 4A).
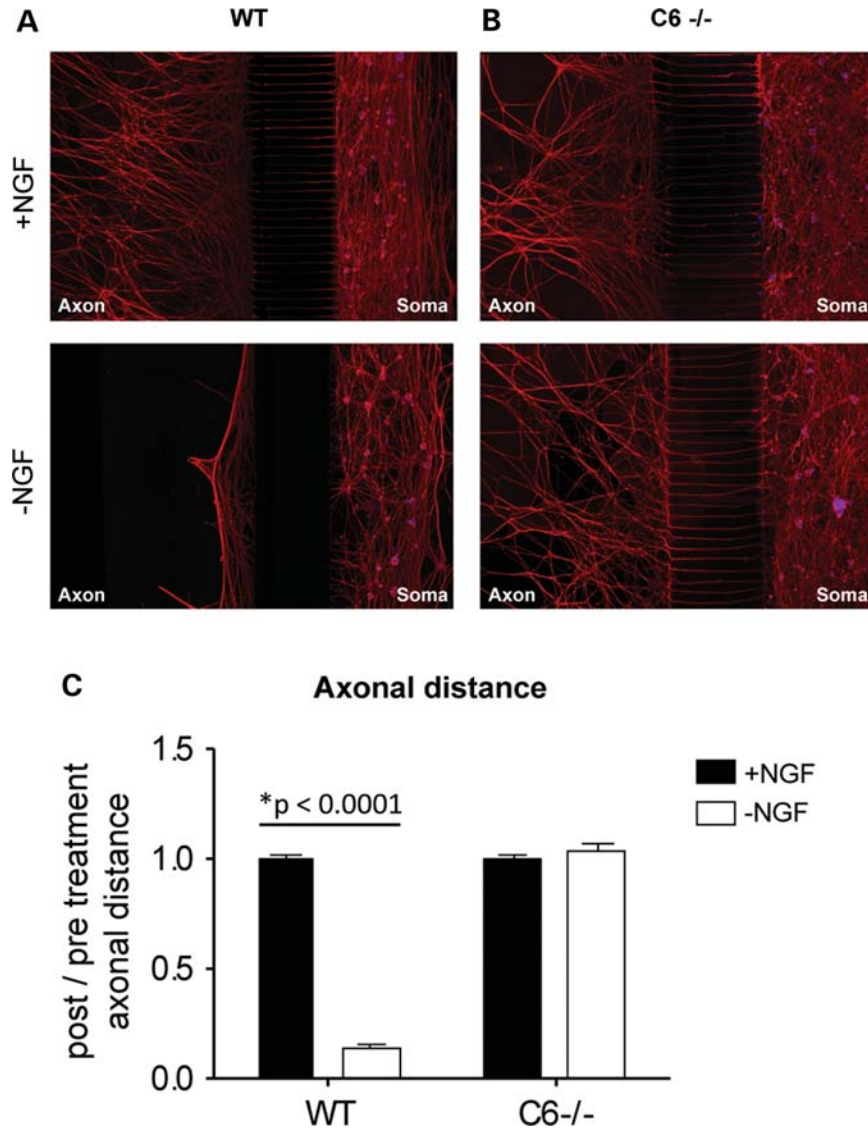
Figure 2. *Casp6−/−* sympathetic neurons show protection against axonal degeneration. (**A**) WT axons from sympathetic neurons grown in microfluidic chambers degenerate after NGF deprivation; in contrast, (**B**) NGF deprivation does not induce degeneration in axons from *Casp6−/−* mice. (**C**) Quantification of axonal distance reveals a significant difference between control and NGF-deprived axons from WT mice (*$P < 0.0001$) and no difference in the axons from *Casp6−/−* mice regardless of treatment conditions ($n = 3$ chambers/condition/genotype).

Cortical and striatal volume is increased in older *Casp6−/−* mice

Mendelian ratios and necropsy were examined prior to neuro-anatomical studies to assess viability and gross peripheral abnormalities in *Casp6*-deficient mice. *Casp6−/−* mice are viable, breed normally and are born in appropriate Mendelian ratios (Supplementary Material, Table S1). Additionally, necropsy performed on *Casp6−/−* mice revealed that the testis, kidney, liver, heart, spleen, stomach, intestine, cecum and colon of the *Casp6−/−* mice are normal compared with WT mice (data not shown; $n = 1$).

Deletions of specific caspases can result in robust brain malformations associated with supernumerary cells, multiple cerebral indentations and ectopic cell masses in the cortex (48–51). To determine whether *Casp6−/−* mice have any

brain malformations, brain and cerebellum weights were measured and more detailed structural and volumetric analyses were examined through stereology in *Casp6−/−* mice at 3 and 8 months of age. *Casp6−/−* mice display normal brain architecture at 3 months of age (Supplementary Material, Fig. S2; one-way ANOVA cortical volume $P = 0.49$, striatal volume $P = 0.66$, striatal neuronal counts $P = 0.23$, brain weight $P = 0.10$, cerebellum weight $P = 0.50$, $n = 20$). However, neuropathological analysis at 8 months reveals a significant increase in cortical (Fig. 5A; one-way ANOVA $P = 0.004$, *post hoc* Tukey WT versus *Casp6−/−* and *Casp6+/−* versus *Casp6−/−* $P < 0.05$, $n = 6$) and striatal volume (Fig. 5A; one-way ANOVA $P = 0.02$, *post hoc* Tukey WT versus *Casp6−/−* $P < 0.05$, $n = 6$) and in striatal neuronal counts (Fig. 5A; one-way ANOVA $P = 0.03$, *post hoc* Tukey WT versus *Casp6−/−* $P < 0.05$, $n = 6$).
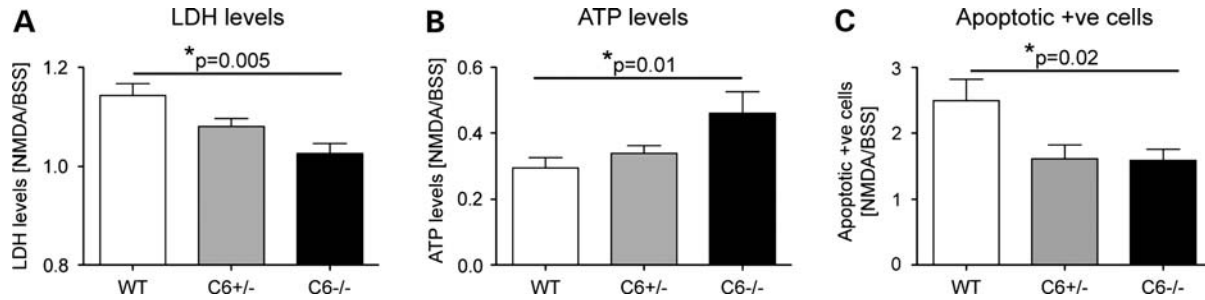
Figure 3. MSNs from *Casp6+/−* and *Casp6−/−* mice show protection against NMDA-mediated excitotoxicity in a Casp6-dose-dependent manner. Assessment of susceptibility to excitotoxic stress demonstrates (**A**) a significant decrease in LDH levels ($n = 10$ cultures/genotype), (**B**) a significant increase in levels of ATP ($n = 10$ cultures/genotype) and (**C**) a significant decrease in number of TUNEL-positive cells ($n = 9–12$ cultures/genotype) in *Casp6−/−* MSNs compared with WT post-NMDA stimulation. *Post hoc* linear trend tests reveal a dose-dependent effect; partial rescue from NMDA is observed in *Casp6+/−* mice (LDH: $P = 0.005$; ATP: $P = 0.01$; TUNEL: $P = 0.02$).

Furthermore, *post hoc* test for linear trend reveals a dose-dependent effect; the *Casp6+/−* mice demonstrate an increase in cortical and striatal volume and in striatal neuronal counts compared with WT, but to a lesser extent than the *Casp6−/−* mice (*post hoc* linear trend, cortex volume: $P = 0.001$; striatum volume: $P = 0.006$; striatal neuronal counts: $P = 0.01$). However, no differences were observed in brain (Fig. 5B; one-way ANOVA $P = 0.36$, $n = 20$) and cerebellum weight (Fig. 5B; one-way ANOVA $P = 0.38$, $n = 20$) in *Casp6−/−* mice compared with WT at 8 months of age.

Casp6−/− mice demonstrate a hypokinetic phenotype and decreased novel object preference

Before conducting behavioral tests, we investigated body weight in *Casp6−/−* mice. Longitudinal recording of body weight shows no differences in body weight between *Casp6−/−* and WT mice from 2 to 8 months of age (females: RM ANOVA genotype: $P = 0.40$, age: $P < 0.0001$, interaction: $P = 0.95$, $n = 7$ WT, 9 *Casp6−/−*; males: RM ANOVA genotype: $P = 0.20$, age: $P < 0.0001$, interaction: $P = 0.42$, $n = 4$ WT, 10 *Casp6−/−*).

In light of the neuroanatomical data, rotarod, total activity and object recognition tasks were conducted to elucidate whether *Casp6−/−* mice show behavioral deficits. Two independent cohorts were tested for each behavioral task, and since the results from the cohorts were not significantly different for each test (ANOVA $P > 0.05$), the cohorts were pooled, analyzed and presented below.

Casp6-deficient mice display motor coordination indistinguishable from WT mice during the accelerating rotarod testing at all time-points assessed (Fig. 6A; factorial ANOVA genotype: $P = 0.27$, age: $P < 0.0001$, interaction: $P = 0.86$, $n = 19$ WT, 21 *Casp6−/−*). However, *Casp6−/−* mice are hypoactive compared with WT mice during the 30 min open-field trial that measures locomotor activity (Fig. 6B; factorial ANOVA genotype: $P = 0.0017$, age: $P = 0.053$, interaction: $P = 0.75$, $n = 17$ WT, 20 *Casp6−/−*).

Furthermore, *Casp6−/−* mice display a deficit in the novel object preference task when tested at 12 months (Fig. 6C; factorial ANOVA genotype: $P = 0.37$, trial: $P < 0.0001$, interaction: $P = 0.0014$, $n = 13$ WT, 19 *Casp6−/−*). In trial 2, WT animals spend more time exploring the novel object that was not present during trial 1 (Fig. 6C; *post hoc* Tukey $P = 0.00016$), indicating that they are able to distinguish the known object from the novel one. However, Casp6-deficient mice did not spend significantly more time exploring the novel object during trial 2 (Fig. 6C; *post hoc* Tukey $P = 0.58$), indicative of a learning deficit at this time-point.

DISCUSSION

In this study, we provide evidence that Casp6 activity *in vivo* is essential for axonal degeneration, as *Casp6−/−* neurons are completely protected from NGF-deprivation-induced axonal loss *in vitro* and do not undergo axonal degeneration on the myelin *in vivo*. We further establish a role of Casp6 in NMDAR-mediated excitotoxic cell death by demonstrating that *Casp6−/−* and *Casp6+/−* neurons are protected against NMDA stimulation in a dose-dependent manner. In addition, this study is the first to examine the neuroanatomical and behavioral effects of ablating Casp6 in mice, which has identified age-dependent and region-specific changes in *Casp6−/−* mice.

Previous studies have demonstrated increased activity of Casp6 in neurological diseases, including HD, AD and ischemia (13–15,23,31,32). Casp6 inhibitors and/or dominant-negative inhibition of Casp6 have also suggested a role for Casp6 in axonal degeneration (31,39).

Axonal degeneration is a key mechanism involved in developmental axonal pruning (41,42). However, it also occurs in the mature nervous system as a consequence of neuronal damage and contributes to neuronal loss in neurodegenerative disorders (31,43,44). Patients with early HD display markedly altered white matter in the corpus callosum, thalamus, sensorimotor and prefrontal regions (45,46,52). Interestingly, white matter pathways of the sensorimotor cortex and corpus callosum are already reduced in pre-manifest HD subjects compared with control subjects (46), indicating that axonal degeneration is an early pathogenic event.

Magnetic resonance imaging analysis of the YAC128 full-length mouse model of HD shows progressive white matter loss that corresponds to alterations observed in human HD (53). Axonal white matter is also reduced in AD patients at the earliest stages of disease (47). Similarly, AD mouse models show age-dependent axonal degeneration in the
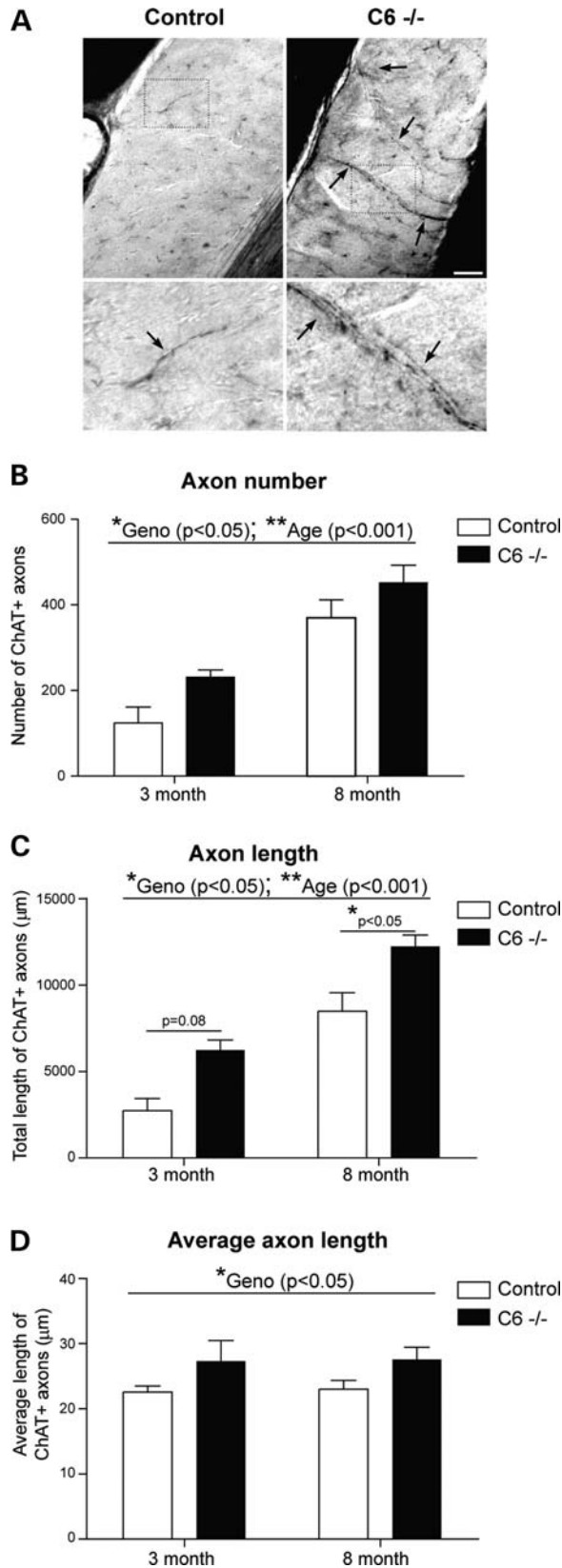
Figure 4. Casp6 is necessary for myelin-dependent axon degeneration *in vivo*. (**A**) Sagittal sections through the corpus callosum and the adjacent supracallosal pathway of adult control and *Casp6−/−* mice immunostained for ChAT. Arrows denote ChAT-positive axons projecting into the corpus callosum, and the boxed areas in the top panels denote regions of the corpus callosum that are shown at higher magnification in the lower panels. Scale bar: 100 μm. Quantification of the number (**B**), length (**C**) and average length (**D**) of ChAT-positive axons projecting vertically into the corpus callosum anterior to the splenium in control versus *Casp6−/−* mice. Error bars represent standard error of the mean. ANOVA: *Geno $P < 0.05$, **Age $P < 0.001$; *Post hoc* Tukey: *$P < 0.05$; $n = 3-4$ each.

cortex, hippocampus, midbrain and hindbrain that likely contributes to the motor and cognitive behavioral deficits observed in these mice (54,55). In an AD mouse model, axonal degeneration occurs through the activation of Casp6 (31,39,56), where the N-terminal fragment of cleaved APP binds to DR6, activating Casp6 and resulting in axonal degeneration (31). The use of Casp6 inhibitors rescued the APP-induced axonal degeneration, thereby implicating a critical role for Casp6 in this process. Casp6 activation also leads to neurite degeneration in a process independent of amyloid β-peptide (Aβ) production from APP cleavage. APP mutants that cannot generate Aβ still induced neurite beading and cell death, which are inhibited by Casp6 inhibitors (56).

It has also been established that Casp6 is involved in focal non-pathogenic axonal pruning along myelin tracks, such as in the corpus callosum, in mice (39). Our findings show that *Casp6−/−* sympathetic neurons are protected against NGF-deprivation-mediated axonal degeneration *in vitro* and *Casp6−/−* cholinergic neurons are protected from pruning of their axons on the myelin-rich corpus callosum *in vivo*. These data are consistent with Casp6 being necessary for myelin-dependent axon degeneration in the intact adult brain.

Casp6 activity has been shown to be increased in the brains of both early stage HD patients and in an HD mouse model (14). In addition to axonal degeneration, we examined whether Casp6 activity may play an important role in NMDAR-induced excitotoxicity. Over-activation of glutamate receptors is involved in the early stages of HD (57,58) and several HD mouse models demonstrate enhanced susceptibility to glutamate and/or NMDAR-mediated excitotoxic stress (14,57,59,60). The direct link between Casp6 activity and enhanced NMDAR-mediated excitotoxic stress in HD mouse models was demonstrated when MSNs expressing mhtt showed Casp6 activation post-NMDA stimulation (14), and protection against excitotoxic stress was observed with use of Casp6 inhibitors and/or dominant negative inhibition of Casp6 (14,15). Furthermore, mice expressing mhtt resistant to cleavage by Casp6 do not show enhanced Casp6 activation and demonstrate protection from excitotoxic stress (14,32) and alterations in extrasynaptic NMDA receptors *in vivo* (35).

To further demonstrate that Casp6 has a crucial role in this process, here we show that MSNs derived from *Casp6+/−* and *Casp6−/−* mice show protection against NMDAR-mediated excitotoxicity in a Casp6-dose-dependent manner. The Casp6 dosage effect suggests that even partial inhibition of Casp6 activity can be beneficial in reducing cell death under excitotoxic conditions. This has important implications for the potential therapeutic efficacy of Casp6 inhibitors in neurological diseases where enhanced susceptibility to NMDAR-mediated excitotoxicity has been shown. Our findings provide further support that inhibition of Casp6 may
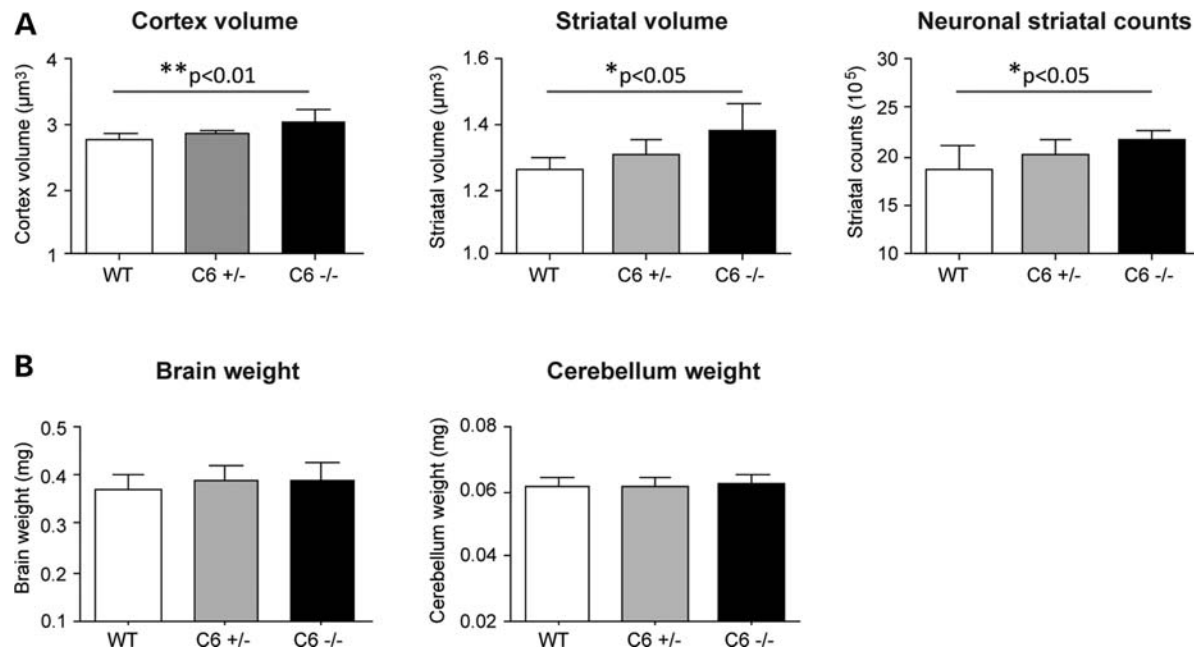
Figure 5. Cortical and striatal volume is increased in 8-month-old *Casp6*−/− mice. Neuropathological analysis at 8 months reveals (**A**) a significant increase in cortical ($n = 6$/genotype) and striatal ($n = 6$/genotype) volume and in striatal neuronal counts ($n = 6$/genotype). *Post hoc* linear trend test reveals a dose-dependent effect; the *Casp6*+/− mice demonstrate an increase in cortical and striatal volume and in striatal neuronal counts compared with WT, but to a lesser extent than the *Casp6*−/− mice (*post hoc* linear trend, cortex volume: $P = 0.001$; striatum volume: $P = 0.006$; striatal neuronal counts: $P = 0.01$). However, no differences are observed in (**B**) brain ($n = 20$/genotype) and cerebellum ($n = 20$/genotype) weight in *Casp6*−/− mice compared with WT. **ANOVA $P < 0.01$; *ANOVA $P < 0.05$.

represent a possible therapeutic target for neurodegenerative diseases (37).

Given the importance of Casp6 in axonal degeneration and excitotoxicity, both processes involved in HD and AD, *Casp6*−/− mice were examined for neuroanatomical alterations in regions affected in these neurodegenerative diseases. Interestingly, we identified age-dependent and region-specific neuroanatomical changes in the *Casp6*−/− mice. Neuroanatomical analysis at 8 months of age reveals a significant increase in cortical and striatal volume and striatal neuronal counts in Casp6-deficient mice compared with WT mice, which were not observed at 3 months of age. Since increased Casp6 activity is implicated in the pathogenesis of HD and AD, where selective degeneration of neuroanatomical structures is progressive and becomes more severe and widespread with advancing age (61–63), the age-dependent increase in cortical and striatal volume observed in *Casp6*−/− mice is congruent with evidence showing that Casp6 is required in processes leading to neurodegeneration. The neuroanatomical alterations observed in *Casp6*-deficient mice also provide evidence that specific brain regions, such as the striatum and cortex, are particularly sensitive to Casp6 activity in an age-dependent manner.

Casp6 does not act alone and plays a crucial role in the regulation of cell death pathway members. Although details of apoptosis pathways are currently being elucidated, Casp9, 3 and 8 are shown to be key regulators and effectors of Casp6 activity (23,64). Casp6 has recently been identified as a downstream target of active Casp9, where inhibition of Casp9 activity results in a lack of Casp6 activation and

protects against ischemic insult (23). Active Casp6 can then initiate cell death pathways by activating Casp3 and 8 (64,65). Casp3 has been implicated in cell death; however, during axonal pruning, Casp6 can activate Casp3 without inducing cell death (31). Since Casp6 signals through other caspases in the apoptosis and axonal pruning pathways, the expression profiles of Casp6 and other caspases in the brain may contribute to the region-specific neuroanatomical changes observed in *Casp6*−/− mice. Casp6 expression is observed predominantly in neurons, with higher expression in MSNs in the striatum, compared with neurons in the cortex, hippocampus and cerebellum (13–15,20,66,67) (Allen Brain Atlas). Striatal MSNs also show high Casp7 expression compared with other brain regions, such as the cortex. Interestingly, Casp7, in the absence of Casp3, can also functionally compensate and ameliorate brain phenotypes seen in Casp3-null mice (51). Unlike Casp6, Casp3 expression is mostly expressed in glia (15), whereas Casp9 is detected in cholinergic neurons and in pyramidal cells located in cortical layer V, and Casp8 is ubiquitously expressed in different brain regions. Therefore, a potential mechanism leading to initial region-specific neurodegeneration in HD and AD could potentially be caused by the regional and selective expression of Casp6 and its interaction with other caspases involved in regulating cell death.

Caspase activation can also be regulated by neurotrophic factors (68). For example, deprivation of brain-derived neurotrophic factor (BDNF) has been shown to trigger cell death pathways by activating caspases through increased p75NTR signaling (69). The presence of BDNF provides protection
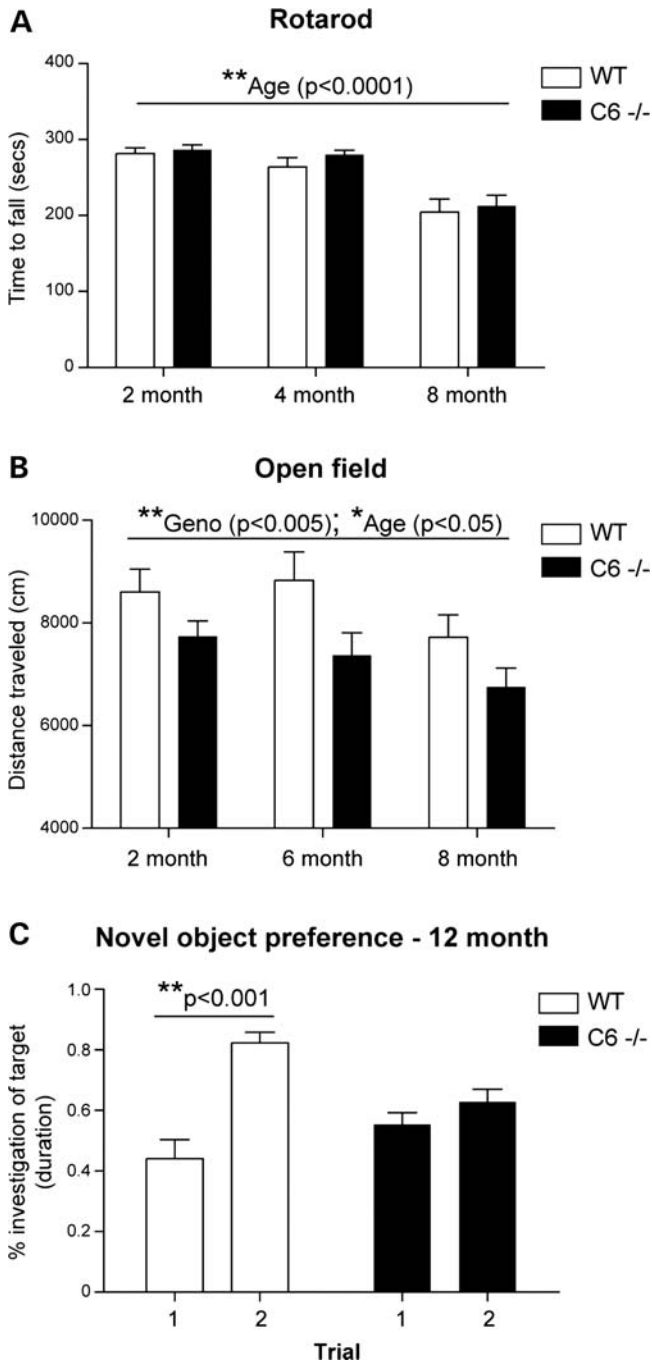
Figure 6. *Casp6*−/− mice demonstrate normal motor coordination, a hypokinetic phenotype and decreased novel object preference. (**A**) *Casp6*−/− mice display motor coordination indistinguishable from WT mice during rotarod testing at all time-points assessed ($n = 19$ WT, 21 *Casp6*−/−). (**B**) *Casp6*−/− mice are hypoactive compared with WT during a 30 min open-field trial (ANOVA: **Geno $P < 0.005$, *Age, $n = 17$ WT, 20 *Casp6*−/−). (**C**) *Casp6*−/− mice demonstrate a deficit in a novel object preference task at 12 months of age (*Post hoc* Tukey $P < 0.001$, $n = 13$ WT, 19 *Casp6*−/−).

against staurosporine-induced excitotoxic cell death *in vitro* by activating the PI3K/Akt pathway through Trk receptor signaling (70). BDNF has also been implicated in neuronal maturation, axonal and dendritic branching and regeneration, and

in synaptic transmission and plasticity (71–73). Although the pathways by which BDNF affects these processes are still being elucidated, BDNF is known to regulate transcription of Sprouty proteins, which modulate neuronal differentiation and survival and axonal branching by inhibiting BDNF signaling in a negative feedback loop (74,75). BDNF has also been shown to play a key role in cognition and behavior by modulating learning, anxiety and depression-like behaviors (76–78). Interestingly, similar to *Casp6*−/− mice, *Bdnf*−/− mice also show structure-specific neuroanatomical alterations and behavioral abnormalities. They display decreased dendritic complexity and spine density in the cortex and hippocampus and to an even greater extent in the striatum, where 90% of the affected cells are GABAergic MSNs (79,80). Behavioral changes associated with BDNF are also region-dependent, and infusion of BDNF in the hippocampal dentate gyrus reduces depression-like behaviors (81); however, infusion into the nucleus accumbens increases depression (82) and social aversion (83). These findings suggest that the diverse responses to BDNF and/or Casp6 by different brain structures may be mediated by region-intrinsic programs (79).

We further examined *Casp6*−/− mice using behavioral tests to elucidate whether the neuroanatomical alterations observed could result in cognitive changes. *Casp6*−/− mice are hypoactive compared with WT mice during a 30 min open-field test that measures locomotor activity. Striatal damage by the neurotoxin 1-methyl-4-phenyl-1,2,3,6-tetrahydropyridine (MPTP) has been shown to impair performance in an open-field test, causing severe behavioral inactivity in distance and speed of locomotion, peripheral activity and frequency and duration of rearing (84). Interestingly, hypoactivity is also observed in the full-length YAC HD mouse model, where degeneration of the striatum is a key pathogenic feature (61,62). These findings suggest that the striatum may be involved in planning and executing pathways of movement. We also show that by 12 months, *Casp6*−/− mice demonstrate a deficit in the novel object recognition task. Excitotoxic lesions of the perirhinal cortex have been shown to cause deficits in object recognition tasks (85,86). Furthermore, studies of neuronal activation in rats and monkeys suggest that cortical neurons are involved in object recognition tasks (87,88). Interestingly, AD mouse models also show age-dependent cortical neuron pathology and deficits in object recognition tasks (89–91), and intrastriatal quinolinic acid injection in mice, which is an acute, *in vivo* HD model, also causes object recognition impairment (92). Altogether, these data suggest that the altered cortical and striatal volume observed in the Casp6-deficient mice could compromise the normal function of these brain regions, and that these changes could possibly translate into the learning impairment and hypoactivity phenotype observed in the *Casp6*−/− mice.

Our data show that the behavioral and neuroanatomical alterations observed in the *Casp6*−/− mice are age dependent. This is consistent with data showing active Casp6 in striatal and cortical neurons of WT mice starting at 9 and 12 months, respectively, with increased activation at 18 months of age. Microarray studies on the cortex and hypothalamus of BALB/c mice also show that Casp6 is significantly up-regulated with age (93), and age-related activation of Casp6 is also observed in human brain tissue (14).

The normal age-dependent activation of Casp6 may explain the neuropathological phenotype observed in the *Casp6−/−* mice, which only manifests with advanced age. Ablating Casp6 while it is predominantly inactive may not cause any brain alterations. However, its absence during a time when Casp6 normally becomes activated could cause a decrease in apoptosis and enlarged brain structures.

Our data highlight the importance of assessing whether Casp6 inhibitors may offer protection against excitotoxic stress and axonal degeneration in neurodegenerative diseases, such as HD and AD. Although detrimental neuropathology is only observed later in life, we have not yet ruled out whether Casp6 deficiency during embryogenesis or development may contribute to the behavioral abnormalities observed in Casp6-deficient mice. Future studies with a conditional Casp6-deficient mouse would allow examination of the morphological and behavioral impact of Casp6 deletion not only in specific brain structures, but also at specific time-points.

MATERIALS AND METHODS

Generation of mutant *Casp6−/−* mice

The *Casp6−/−* mouse was created by Taconic Biosciences by targeted gene disruption of Casp6 gene in embryonic stem cells. Exons 2–5 of the *Casp6* gene, which encode the catalytic domain of the Casp6 protein, were disrupted in embryonic stem cells by homologous recombination to generate *Casp6−/−* mice (Supplementary Material, Fig. S1A and B). The homologous recombination strategy was validated by Southern analysis. Two PCR assays were designed for genotyping: the WT assay amplifies the WT allele from *Casp6* WT and heterozygous (*Casp6+/−*) mice; and the mt allele assay amplifies the knocked out allele from *Casp6+/−* and *Casp6−/−* mice. The following primers were used:

- WT assay forward: 5′-AGGGTGGGTTAGACCAGG TT-3′;
- WT assay reverse: 5′-TCCAGCTTGTCTGTCTGGT G-3′;
- mt assay forward: 5′-CCTGTGGGGTCAAAAGACTT TCACAG-3′;
- mt assay reverse: 5′-GCAAGCTGCTAACAGCCAA CACAAC-3′.

The PCR was performed in a 20 μl volume, using 1.5 μl of genomic DNA in 10× PCR buffer, 50 mM MgCl$_2$, 10 mM dNTP, 2% formamide, 50% glycerol, Taq polymerase and DH$_2$O. A complex temperature profile was adopted to ensure maximum specificity in the early rounds of amplification. An initial DNA denaturation for 3 min at 94°C was followed by 35 cycles at 94°C for 30 s, 60°C for 1 min, 72°C for 1 min and finally a 7 min extension at 72°C.

Breeding and housing

The *Casp6* knockout mouse, originally generated on the C57Bl/6 (B6) strain, was backcrossed for five generations to the FVB/NJ (FVB) strain. All the experiments, with the exception of the necropsy and the Mendelian ratios, which were performed and the data recorded on both the B6 and FVB strains, were conducted on the incipient congenic mice on the FVB strain and according to the protocols approved by the University of British Columbia Committee on Animal Care (protocol A07-0106). The mice were housed in groups of maximum five mice per cage as previously described (61).

mRNA analysis and qRT-PCR

RNA was extracted from *Casp6−/−* and WT mice whole brain using the RNeasy Mini Kit (Qiagen, 74104). cDNA was prepared using 250 ng of total RNA and the Superscript-III First-Strand Synthesis Kit with oligo-dT priming (Invitrogen, 11752-050). SYBR Green PCR Master Mix (Applied Biosystems, 4309155) in the ABI7500 instrument was used to perform the quantitative real-time PCR with the absolute quantification standard curve method. The following primers were used:

- mouse Casp6 forward: 5′-CAACGCAGACAGAGACA ACCT-3′;
- mouse Casp6 reverse: 5′-TCGACACCTCGTGAATTT TGAG-3′;
- mouse actin forward: 5′-ACGGCCAGGTCATCACTA TTG-3′;
- mouse actin reverse: 5′-CAAGAAGGAAGGCTGGA AAAGA-3′.

Protein analysis and western blotting

Protein was extracted as previously described (94) from brain and peripheral tissues from *Casp6−/−* and WT mice and its concentration measured by Bio-Rad DC Protein Assay. Four to 12% Bis–Tris polyacrylamide gels from Invitrogen were used to load 70 μg of protein for brain and peripheral tissues in LDS sample buffer (Invitrogen, NP0008) after it was denatured by heating it to 70°C. Proteins were transferred to an Immobilon-PVDF-FL membrane and probed with a Casp6 antibody (Cell Signaling 9762, 1:500) and calnexin antibody (Sigma C4731, 1:5000).

Necropsy

Kidney, liver, heart, spleen, stomach, intestine, cecum, colon and testis tissues were collected from one B6 *Casp6−/−* mouse and one FVB *Casp6−/−* mouse, and stored in 10% formalin. A #15 scalpel blade was used to cut the tissues into 3–4 mm sections; they were placed into cassettes and then set in a paraffin block and cut into 1 μm slices using a microtome. They were mounted into slides and a hematoxylin and eosin stain was applied in order to perform a macroscopic examination of the different tissues cell structure.

NMDAR-mediated excitotoxicity

Cultures (9–12 individual cultures) of primary MSNs were prepared from P0–P1 *Casp6−/−* and WT pups in a

procedure described previously (32,58). Cultures were maintained *in vitro* for 9–10 days, after which they were exposed to balanced salt solution (BSS) or 500 μm NMDA (Sigma) in BSS for 10 min. Twenty-four hours after NMDA, cultures were fixed and assessed for apoptotic cell death using TUNEL staining (Roche) and morphological criteria (small, condensed nuclei) by propidium iodide (Sigma) counterstaining. For each experiment, all treatments were done blind, in triplicate, and a minimum of 1000 cells counted.

LDH and ATP were assessed in separate cultures. Twenty-four hours after stress, 50 μl of culture media were used for LDH quantification, according to the manufacturer's instructions (Roche, Cytotoxicity Detection Kit). For ATP assessment, CellTiter-Glo Luminescent Cell Viability Assay from Promega was used. Cells were lysed on an orbital rotator at room temperature for 10 min. One hundred microliters of cell lysis was removed to a black 96-well plate and luminescence recorded with PolarStar Omega plate reader. In order to obtain the LDH and ATP data, the raw value of each well was normalized to BSS-treated cells/neurons on the same plate.

NGF-induced axonal degeneration in microfluidic chambers

Sympathetic neurons were isolated as previously described (95) from P0–P1 WT and *Casp-6* −/− mice. Briefly, PDMS (Sylgard 183, Dow Corning) replica-molded microfluidic chambers (96) were placed onto glass cover slips coated with poly-D-lysine (50 μg/ml) and laminin (1 μg/ml). Dissociated sympathetic cervical ganglion neurons (approximately 20 000 cells) were plated into the somatic compartment and maintained in NGF-containing (50 ng/ml) media for 5–6 days. For localized NGF deprivation, the axon compartment was rinsed three times with medium lacking NGF and then maintained in 70 μl of NGF-free media containing an anti-NGF-neutralizing antibody. One hundred liters of NGF-containing media remained in the somatic compartment to create a 30 μl volume differential between the two compartments. The volume differential was carefully maintained during local deprivation to prevent any medium exchange between soma and axon compartments.

Fixed neurons were then probed with tubulin (Sigma T9026, 1:400), using standard immunofluorescence techniques. Nuclei were stained with Hoechst 33258 (Molecular Probes). Images were acquired by an ORCA-ER digital B/W CCD camera (Hamamatsu) mounted on a DMIRE2 inverted fluorescence microscope (Leica), using the Metamorph version 7.6 software (Molecular Devices). Adobe Photoshop was used to scale down and crop images to prepare the final figures.

The Metamorph version 7.6 software was used to measure horizontal axon distance (μm) from the left outer edge of the central channels (where the axons exit the channels and enter the axon compartment) to the farthest point of axon growth inside the axon compartment. Unbiased measurements were obtained by measuring axon distance at every sixth channel within the same chamber both before and after treatment. To calculate fold change, the mean post-treatment axon distance was divided by the mean pre-treatment axon distance. Fold change in axon distance was calculated for three

chambers per condition. Graph values represent the average fold change in axon distance ± standard error of the mean (SEM) ($n = 3$).

Stereology

Quantitative analysis was done blind to genotype. Mice were terminally anesthetized by intra-peritoneal injection of 2.5% avertin and perfused with 3% paraformaldehyde/0.15% glutaraldehyde in phosphate-buffered saline (PBS). Mouse brains were post-fixed in the same solution for 24 h at 4°C and then cryoprotected in 30% sucrose prior to coronal sectioning on a cryostat (MICROM HM 500 M, MICROM, Heiderberg, Germany) at 25 μm. Every eighth section throughout the striatum from the bregma (1.34 to −0.94 mm) was collected and stained with an antibody reactive to NeuN (Chemicon), a marker of neuronal nuclei (93), as described previously (61).

The area of the striatum was traced with the Stereoinvestigator 10.0 software (Microbrightfield, Williston, VT, USA). For neuronal counts, the physical fractionator probe was used with a grid size of 500×500 and counting frame of 25×25 and the nucleator probe was used for the measurement of neuronal size. A minimum of 200–300 cells per animal were counted and analyzed. For striatal volume, the Cavalieri principle was employed where the total striatal area was multiplied by section thickness (25 μm) and sectional sampling interval (8) as previously described (97,98) ($n = 20$/genotype at 3 months, $n = 6$/genotype at 8 months). The cortex was delineated using the corpus callosum as the ventral boundary in the same sections used for striatal analyses. Cortical volume was determined according to the Cavalieri principle as previously described (97,98) ($n = 20$/genotype at 3 months, $n = 6$/genotype at 8 months).

For analysis of cholinergic axons in the CNS, adult mice were anesthetized, intracardially perfused with ice-cold 0.9% NaCl and fixed with 4% paraformaldehyde (Electron Microscopy Sciences). Brains were post-fixed for 6 h in 4% paraformaldehyde at 4°C and cryoprotected in 30% (w/v) sucrose in PBS, and sagittal serial 40 μm sections were collected in cryoprotectants. For diaminobenzidine staining, we analyzed every third section from 0–480 μm away from the midline, using standard immunohistochemical procedures (39). Briefly, sections were rinsed three times for 10 min each in TBS, incubated in 0.6% H_2O_2 for 15 min and blocked in Tris buffer containing 5% donkey serum and 0.25% Triton X-100. Sections were incubated overnight at 4°C in primary antibody, anti-ChAT (1:200, Chemicon), diluted in blocking solution. Sections were rinsed three times for 10 min each in TBS and incubated with a biotinylated donkey-anti-goat secondary antibody for 2 h at room temperature. Sections were then rinsed and processed with avidin–biotin complex (Vectastain Elite, Vector Laboratories) and 3′,3′-diaminobenzidine (Vector). Sections were rinsed, mounted onto gelatin-coated glass slides, dried overnight, dehydrated in an alcohol gradient, washed in xylene and cover-slipped using Permount (Fisher). For immunofluorescence staining, random sections from 0–480 μm away from the midline were rinsed three times for 10 min each in PBS, blocked in PBS containing 10% donkey serum, 2% horse serum and 0.25% Triton X-100, incubated overnight at 4°C in blocking solution plus

primary antibody, rinsed three times for 10 min each in PBS, incubated with secondary antibody for 2 h at room temperature, rinsed and mounted using Fluoromount (Sigma-Aldrich) ($n = 3–4$/genotype at 3 and 8 months).

Body weight

Mice were weighed at 2, 4, 6 and 8 months of age using a digital scale and weight recorded. Female: WT ($n = 7$) and *Casp6*−/− ($n = 9$). Male: WT ($n = 4$) and *Casp6*−/− ($n = 10$).

Behavior

Behavioral analysis of *Casp6*−/− and WT mice was done blind to genotype.

Rotarod

Motor coordination and learning were examined using an accelerating rotarod (UGO Basile, Comerio, Italy). For training, naïve 2-month-old mice were given three trials of 2 min on a fixed speed (18 r.p.m.) task per day for three days (nine trials total). The inter-trial interval (ITI) was 2 h. Mice falling from the rod were returned, to a maximum of 10 falls/trial. The time to first fall and the total number of falls per trial were recorded. For accelerating rotarod assessment, mice were tested at 2, 4 and 8 months of age on a rod accelerating from 5 to 40 r.p.m. for 300 s. Latency to fall from the rod was recorded. Three trials in 1 day were averaged to give mean performance for each mouse at each age ($n = 19$ WT, 21 *Casp6*−/−).

Open-field activity monitoring

Mice ($n = 17$ WT, 20 *Casp6*−/−) were assessed using an open-field activity monitor (Med Associates, Inc., St Albans, VT, USA) during the dark cycle at 2, 6 and 8 months of age. Mice were placed in the testing chamber for 30 min, total activity was recorded and measurements were calculated using the accompanying software (Med Associates). The testing chambers were wiped clean with water between mice.

Novel-object recognition

Mice ($n = 13$ WT, 19 *Casp6*−/−) were placed at the lower left corner of a 50×50 cm² open grey acrylic box with a 20×20 cm center in a room brightly lit by fluorescent ceiling lights. Open-field activity was recorded for 10 min by a ceiling-mounted video camera. Distance traveled, mean velocity, entries into the 20×20 cm² center and time spent in the center of the center point of the mouse were scored using the Ethovision 7.0 XT software (Noldus).

After open-field exploration, which allows acclimation to the testing arena, mice were returned to their home cage for a 5 min ITI. Two different novel objects of sufficient height and weight to prevent mice from moving or climbing on them were placed at the upper two corners of the box, far enough from the sides so as to not impede movement around the outer edge ($\sim$8 cm). Mice were re-introduced into the box at the lower left corner and recorded for 5 min, during which the number of investigations of the objects was scored as frequency and duration of the nose point of the mouse entering the zone immediately around the object, using the Ethovision XT software. Mice were then removed from the box for a 5 min interval, and the object at the top right corner of the box was replaced by a different unfamiliar object in the same location. Mice were re-introduced into the box and recorded for 5 min and the number and duration of investigations of the objects were scored. For novel-object preference testing, the percentage of the investigations to the target object (the unfamiliar one) was computed. For novel-object location, the experiment was repeated on the subsequent day, but rather than replacing the object with an unfamiliar one, the object at the top right corner of the box was moved to the lower right corner of the box. The percentage of the investigations to the target object (the one in the new location) was computed.

Statistics

Statistical analysis (i.e. *P*-values, means and SEMs) was performed using Prism, version 4.0 (GraphPad Software). Differences between means were considered statistically significant if $P < 0.05$.

Axon distance before and after NGF deprivation was measured and fold change was calculated by dividing the mean post-treatment axon distance by the mean pre-treatment axon distance. Fold change in axon distance was calculated for three chambers per condition. Graph values represent the average fold change in axon distance $\pm$ SEM ($n = 3$). An unpaired Student's *t*-test was used to determine whether there was a statistically significant difference between treatment conditions. The *t*-test was also used to analyze the number and length of ChAT-positive axons in the corpus callosum.

Statistical analysis of the LDH, ATP and TUNEL data, as well as of the stereology data, was performed using one-way ANOVA. Significant genotype effects were followed up with *post hoc* Tukey comparisons and *post hoc* linear trend tests. Statistical analysis of the body weight was performed using a repeated-measures ANOVA model. For rotarod data, a factorial ANOVA was used to determine genotype, age and genotype–age interaction effects. Similarly, for the novel-object recognition test, a factorial ANOVA was used to determine genotype, trial and genotype–trial interaction effects. Significant effects were followed by *post hoc* Tukey comparison test.

SUPPLEMENTARY MATERIAL

Supplementary Material is available at *HMG* online.

AUTHORS' CONTRIBUTIONS

V.U., R.K.G. and M.R.H. designed research; V.U., B.K.Y.W., R.K.G., C.L.C., N.H.S., M.A.P., Y.X., K.F., Y.O., Y.O., Y.D., D.E.E., S.F., N.G., A.S., W.Z. and K.V. performed research; V.U., B.K.Y.W., R.K.G., C.L.C., K.F., Y.O. and Y.O. analyzed data; and V.U., B.K.Y.W. and F.D.M wrote the paper with guidance from R.K.G. and M.R.H. All authors contributed to editing.

REFERENCES

1. Arends, M.J. and Wyllie, A.H. (1991) Apoptosis: mechanisms and roles in pathology. *Int. Rev. Exp. Pathol.*, **32**, 223–254.
2. Ellis, R.E., Yuan, J.Y. and Horvitz, H.R. (1991) Mechanisms and functions of cell death. *Annu. Rev. Cell Biol.*, **7**, 663–698.
3. Zheng, T.S. and Flavell, R.A. (1999) Apoptosis. All's well that ends dead. *Nature*, **400**, 410–411.
4. Zheng, T.S., Hunot, S., Kuida, K. and Flavell, R.A. (1999) Caspase knockouts: matters of life and death. *Cell Death Differ.*, **6**, 1043–1053.
5. Raff, M.C., Barres, B.A., Burne, J.F., Coles, H.S., Ishizaki, Y. and Jacobson, M.D. (1993) Programmed cell death and the control of cell survival: lessons from the nervous system. *Science*, **262**, 695–700.
6. Troy, C.M. and Salvesen, G.S. (2002) Caspases on the brain. *J. Neurosci. Res.*, **69**, 145–150.
7. De Maria, R., Zeuner, A., Eramo, A., Domenichelli, C., Bonci, D., Grignani, F., Srinivasula, S.M., Alnemri, E.S., Testa, U. and Peschle, C. (1999) Negative regulation of erythropoiesis by caspase-mediated cleavage of GATA-1. *Nature*, **401**, 489–493.
8. Kennedy, N., Kataoka, T., Tschopp, J. and Budd, R.C. (1999) Caspase activation is required for T cell proliferation. *J. Exp. Med.*, **190**, 1725–1728.
9. Li, Z., Jo, J., Jia, J.-M., Lo, S.-C., Whitcomb, D.J., Jiao, S., Cho, K. and Sheng, M. (2010) Caspase-3 activation via mitochondria is required for long-term depression and AMPA receptor internalization. *Cell*, **141**, 859–871.
10. Fischer, U., Jänicke, R.U. and Schulze-Osthoff, K. (2003) Many cuts to ruin: a comprehensive update of caspase substrates. *Cell Death Differ.*, **10**, 76–100.
11. Dash, P.K., Blum, S. and Moore, A.N. (2000) Caspase activity plays an essential role in long-term memory. *Neuroreport*, **11**, 2811–2816.
12. Nicholson, D.W. (1999) Caspase structure, proteolytic substrates, and function during apoptotic cell death. *Cell Death Differ.*, **6**, 1028–1042.
13. Albrecht, S., Bogdanovic, N., Ghetti, B., Winblad, B. and LeBlanc, A.C. (2009) Caspase-6 activation in familial Alzheimer disease brains carrying amyloid precursor protein or presenilin I or presenilin II mutations. *J. Neuropathol. Exp. Neurol.*, **68**, 1282–1293.
14. Graham, R.K., Deng, Y., Carroll, J., Vaid, K., Cowan, C., Pouladi, M.A., Metzler, M., Bissada, N., Wang, L., Faull, R.L.M. *et al.* (2010) Cleavage at the 586 amino acid caspase-6 site in mutant huntingtin influences caspase-6 activation in vivo. *J. Neurosci.*, **30**, 15019–15029.
15. Hermel, E., Gafni, J., Propp, S.S., Leavitt, B.R., Wellington, C.L., Young, J.E., Hackam, A.S., Logvinova, A.V., Peel, A.L., Chen, S.F. *et al.* (2004) Specific caspase interactions and amplification are involved in selective neuronal vulnerability in Huntington's disease. *Cell Death Differ.*, **11**, 424–438.
16. Slee, E.A., Harte, M.T., Kluck, R.M., Wolf, B.B., Casiano, C.A., Newmeyer, D.D., Wang, H.G., Reed, J.C., Nicholson, D.W., Alnemri, E.S. *et al.* (1999) Ordering the cytochrome *c*-initiated caspase cascade: hierarchical activation of caspases-2, -3, -6, -7, -8, and -10 in a caspase-9-dependent manner. *J. Cell Biol.*, **144**, 281–292.
17. D'Amelio, M., Cavallucci, V., Middei, S., Marchetti, C., Pacioni, S., Ferri, A., Diamantini, A., De Zio, D., Carrara, P., Battistini, L. *et al.* (2011) Caspase-3 triggers early synaptic dysfunction in a mouse model of Alzheimer's disease. *Nat. Neurosci.*, **14**, 69–76.
18. Zhang, J., Gorostiza, O.F., Tang, H., Bredesen, D.E. and Galvan, V. (2010) Reversal of learning deficits in hAPP transgenic mice carrying a mutation at Asp664: a role for early experience. *Behav. Brain Res.*, **206**, 202–207.
19. Gervais, F.G., Xu, D., Robertson, G.S., Vaillancourt, J.P., Zhu, Y., Huang, J., LeBlanc, A., Smith, D., Rigby, M., Shearman, M.S. *et al.* (1999) Involvement of caspases in proteolytic cleavage of Alzheimer's amyloid-beta precursor protein and amyloidogenic A beta peptide formation. *Cell*, **97**, 395–406.
20. Albrecht, S., Bourdeau, M., Bennett, D., Mufson, E.J., Bhattacharjee, M. and LeBlanc, A.C. (2007) Activation of caspase-6 in aging and mild cognitive impairment. *Am. J. Pathol.*, **170**, 1200–1209.
21. Kubodera, T., Yokota, T., Ohwada, K., Ishikawa, K., Miura, H., Matsuoka, T. and Mizusawa, H. (2003) Proteolytic cleavage and cellular toxicity of the human alpha1A calcium channel in spinocerebellar ataxia type 6. *Neurosci. Lett.*, **341**, 74–78.
22. Haacke, A., Broadley, S.A., Boteva, R., Tzvetkov, N., Hartl, F.U. and Breuer, P. (2006) Proteolytic cleavage of polyglutamine-expanded ataxin-3 is critical for aggregation and sequestration of non-expanded ataxin-3. *Hum. Mol. Genet.*, **15**, 555–568.
23. Akpan, N., Serrano-Saiz, E., Zacharia, B.E., Otten, M.L., Ducruet, A.F., Snipas, S.J., Liu, W., Velloza, J., Cohen, G., Sosunov, S.A. *et al.* (2011) Intranasal delivery of caspase-9 inhibitor reduces caspase-6-dependent axon/neuron loss and improves neurological function after stroke. *J. Neurosci.*, **31**, 8894–8904.
24. Galvan, V., Gorostiza, O.F., Banwait, S., Ataie, M., Logvinova, A.V., Sitaraman, S., Carlson, E., Sagi, S.A., Chevallier, N., Jin, K. *et al.* (2006) Reversal of Alzheimer's-like pathology and behavior in human APP transgenic mice by mutation of Asp664. *Proc. Natl Acad. Sci. USA*, **103**, 7130–7135.
25. Galvan, V., Zhang, J., Gorostiza, O.F., Banwait, S., Huang, W., Ataie, M., Tang, H. and Bredesen, D.E. (2008) Long-term prevention of Alzheimer's disease-like behavioral deficits in PDAPP mice carrying a mutation in Asp664. *Behav. Brain Res.*, **191**, 246–255.
26. Saganich, M.J., Schroeder, B.E., Galvan, V., Bredesen, D.E., Koo, E.H. and Heinemann, S.F. (2006) Deficits in synaptic transmission and learning in amyloid precursor protein (APP) transgenic mice require C-terminal cleavage of APP. *J. Neurosci.*, **26**, 13428–13436.
27. Nguyen, T.-V.V., Galvan, V., Huang, W., Banwait, S., Tang, H., Zhang, J. and Bredesen, D.E. (2008) Signal transduction in Alzheimer disease: p21-activated kinase signaling requires C-terminal cleavage of APP at Asp664. *J. Neurochem.*, **104**, 1065–1080.
28. Banwait, S., Galvan, V., Zhang, J., Gorostiza, O.F., Ataie, M., Huang, W., Crippen, D., Koo, E.H. and Bredesen, D.E. (2008) C-terminal cleavage of the amyloid-beta protein precursor at Asp664: a switch associated with Alzheimer's disease. *J. Alzheimers Dis.*, **13**, 1–16.
29. Bredesen, D.E., John, V. and Galvan, V. (2010) Importance of the caspase cleavage site in amyloid-beta protein precursor. *J. Alzheimers Dis.*, **22**, 57–63.
30. Harris, J.A., Devidze, N., Halabisky, B., Lo, I., Thwin, M.T., Yu, G.Q., Bredesen, D.E., Masliah, E. and Mucke, L. (2010) Many neuronal and behavioral impairments in transgenic mouse models of Alzheimer's

disease are independent of caspase cleavage of the amyloid precursor protein. *J. Neurosci.*, **30**, 372–381.

31. Nikolaev, A., McLaughlin, T., O'Leary, D.D.M. and Tessier-Lavigne, M. (2009) APP binds DR6 to trigger axon pruning and neuron death via distinct caspases. *Nature*, **457**, 981–989.

32. Graham, R.K., Deng, Y., Slow, E.J., Haigh, B., Bissada, N., Lu, G., Pearson, J., Shehadeh, J., Bertram, L., Murphy, Z. *et al.* (2006) Cleavage at the caspase-6 site is required for neuronal dysfunction and degeneration due to mutant huntingtin. *Cell*, **125**, 1179–1191.

33. Tebbenkamp, A.T., Green, C., Xu, G., Denovan-Wright, E.M., Rising, A.C., Fromholt, S.E., Brown, H.H., Swing, D., Mandel, R.J., Tessarollo, L. *et al.* (2011) Transgenic mice expressing caspase-6-derived N-terminal fragments of mutant huntingtin develop neurologic abnormalities with predominant cytoplasmic inclusion pathology composed largely of a smaller proteolytic derivative. *Hum. Mol. Genet.*, **20**, 2770–2782.

34. Pouladi, M.A., Graham, R.K., Karasinska, J.M., Xie, Y., Santos, R.D., Petersén, A. and Hayden, M.R. (2009) Prevention of depressive behaviour in the YAC128 mouse model of Huntington disease by mutation at residue 586 of huntingtin. *Brain*, **132**, 919–932.

35. Milnerwood, A.J., Gladding, C.M., Pouladi, M.A., Kaufman, A.M., Hines, R.M., Boyd, J.D., Ko, R.W.Y., Vasuta, O.C., Graham, R.K., Hayden, M.R. *et al.* (2010) Early increase in extrasynaptic NMDA receptor signaling and expression contributes to phenotype onset in Huntington's disease mice. *Neuron*, **65**, 178–190.

36. Metzler, M., Gan, L., Mazarei, G., Graham, R.K., Liu, L., Bissada, N., Lu, G., Leavitt, B.R. and Hayden, M.R. (2010) Phosphorylation of huntingtin at Ser421 in YAC128 neurons is associated with protection of YAC128 neurons from NMDA-mediated excitotoxicity and is modulated by PP1 and PP2A. *J. Neurosci.*, **30**, 14318–14329.

37. Leyva, M.J., Degiacomo, F., Kaltenbach, L.S., Holcomb, J., Zhang, N., Gafni, J., Park, H., Lo, D.C., Salvesen, G.S., Ellerby, L.M. *et al.* (2010) Identification and evaluation of small molecule pan-caspase inhibitors in Huntington's disease models. *Chem. Biol.*, **17**, 1189–1200.

38. O'Brien, T. and Lee, D. (2004) Prospects for caspase inhibitors. *Mini Rev. Med. Chem.*, **4**, 153–165.

39. Park, K.J., Grosso, C.A., Aubert, I., Kaplan, D.R. and Miller, F.D. (2010) p75NTR-dependent, myelin-mediated axonal degeneration regulates neural connectivity in the adult brain. *Nat. Neurosci.*, **13**, 559–566.

40. Fernandes-Alnemri, T., Litwack, G. and Alnemri, E.S. (1995) Mch2, a new member of the apoptotic Ced-3/Ice cysteine protease gene family. *Cancer Res.*, **55**, 2737–2742.

41. Raff, M.C., Whitmore, A.V. and Finn, J.T. (2002) Axonal self-destruction and neurodegeneration. *Science*, **296**, 868–871.

42. Buss, R.R., Sun, W. and Oppenheim, R.W. (2006) Adaptive roles of programmed cell death during nervous system development. *Annu. Rev. Neurosci.*, **29**, 1–35.

43. Singh, K.K., Park, K.J., Hong, E.J., Kramer, B.M., Greenberg, M.E., Kaplan, D.R. and Miller, F.D. (2008) Developmental axon pruning mediated by BDNF-p75NTR-dependent axon degeneration. *Nat. Neurosci.*, **11**, 649–658.

44. Luo, L. and O'Leary, D.D.M. (2005) Axon retraction and degeneration in development and disease. *Annu. Rev. Neurosci.*, **28**, 127–156.

45. Rosas, H.D., Lee, S.Y., Bender, A.C., Zaleta, A.K., Vangel, M., Yu, P., Fischl, B., Pappu, V., Onorato, C., Cha, J.H., Salat, D.H. and Hersch, S.M. (2010) Altered white matter microstructure in the corpus callosum in Huntington's disease: implications for cortical disconnection. *Neuroimage*, **49**, 2995–3004.

46. Dumas, E.M., van den Bogaard, S.J., Ruber, M.E., Reilman, R.R., Stout, J.C., Craufurd, D., Hicks, S.L., Kennard, C., Tabrizi, S.J., van Buchem, M.A. *et al.* (2011) Early changes in white matter pathways of the sensorimotor cortex in premanifest Huntington's disease. *Hum. Brain Mapp.*, **33**, 203–212.

47. Salat, D.H., Greve, D.N., Pacheco, J.L., Quinn, B.T., Helmer, K.G., Buckner, R.L. and Fischl, B. (2009) Regional white matter volume differences in nondemented aging and Alzheimer's disease. *Neuroimage*, **44**, 1247–1258.

48. Varfolomeev, E.E., Schuchmann, M., Luria, V., Chiannilkulchai, N., Beckmann, J.S., Mett, I.L., Rebrikov, D., Brodianski, V.M., Kemper, O.C., Kollet, O. *et al.* (1998) Targeted disruption of the mouse Caspase 8 gene ablates cell death induction by the TNF receptors, Fas/Apo1, and DR3 and is lethal prenatally. *Immunity*, **9**, 267–276.

49. Kuida, K., Haydar, T.F., Kuan, C.Y., Gu, Y., Taya, C., Karasuyama, H., Su, M.S., Rakic, P. and Flavell, R.A. (1998) Reduced apoptosis and cytochrome *c*-mediated caspase activation in mice lacking caspase 9. *Cell*, **94**, 325–337.

50. Hakem, R., Hakem, A., Duncan, G.S., Henderson, J.T., Woo, M., Soengas, M.S., Elia, A., de la Pompa, J.L., Kagi, D., Khoo, W. *et al.* (1998) Differential requirement for caspase 9 in apoptotic pathways in vivo. *Cell*, **94**, 339–352.

51. Houde, C., Banks, K.G., Coulombe, N., Rasper, D., Grimm, E., Roy, S., Simpson, E.M. and Nicholson, D.W. (2004) Caspase-7 expanded function and intrinsic expression level underlies strain-specific brain phenotype of caspase-3-null mice. *J. Neurosci.*, **24**, 9977–9984.

52. Paulsen, J.S., Nopoulos, P.C., Aylward, E., Ross, C.A., Johnson, H., Magnotta, V.A., Juhl, A., Pierson, R.K., Mills, J., Langbehn, D. *et al.* (2010) Striatal and white matter predictors of estimated diagnosis for Huntington disease. *Brain Res. Bull.*, **82**, 201–207.

53. Carroll, J.B., Lerch, J.P., Franciosi, S., Spreeuw, A., Bissada, N., Henkelman, R.M. and Hayden, M.R. (2011) Natural history of disease in the YAC128 mouse reveals a discrete signature of pathology in Huntington disease. *Neurobiol. Dis.*, **43**, 257–265.

54. Dawson, H.N., Cantillana, V., Jansen, M., Wang, H., Vitek, M.P., Wilcock, D.M., Lynch, J.R. and Laskowitz, D.T. (2010) Loss of tau elicits axonal degeneration in a mouse model of Alzheimer's disease. *Neuroscience*, **169**, 516–531.

55. Jawhar, S., Trawicka, A., Jenneckens, C., Bayer, T.A. and Wirths, O. (2010) Motor deficits, neuron loss, and reduced anxiety coinciding with axonal degeneration and intraneuronal Abeta aggregation in the 5XFAD mouse model of Alzheimer's disease. *Neurobiol. Aging*, **33**, e29–e40.

56. Sivananthan, S.N., Lee, A.W., Goodyer, C.G. and LeBlanc, A.C. (2010) Familial amyloid precursor protein mutants cause caspase-6-dependent but amyloid β-peptide-independent neuronal degeneration in primary human neuron cultures. *Cell Death Dis.*, **1**, e100.

57. Levine, M.S., Klapstein, G.J., Koppel, A., Gruen, E., Cepeda, C., Vargas, M.E., Jokel, E.S., Carpenter, E.M., Zanjani, H., Hurst, R.S. *et al.* (1999) Enhanced sensitivity to *N*-methyl-D-aspartate receptor activation in transgenic and knockin mouse models of Huntington's disease. *J. Neurosci. Res.*, **58**, 515–532.

58. Zeron, M.M., Hansson, O., Chen, N., Wellington, C.L., Leavitt, B.R., Brundin, P., Hayden, M.R. and Raymond, L.A. (2002) Increased sensitivity to *N*-methyl-D-aspartate receptor-mediated excitotoxicity in a mouse model of Huntington's disease. *Neuron*, **33**, 849–860.

59. Graham, R.K., Slow, E.J., Deng, Y., Bissada, N., Lu, G., Pearson, J., Shehadeh, J., Leavitt, B.R., Raymond, L.A. and Hayden, M.R. (2006) Levels of mutant huntingtin influence the phenotypic severity of Huntington disease in YAC128 mouse models. *Neurobiol. Dis.*, **21**, 444–455.

60. Zeron, M.M., Fernandes, H.B., Krebs, C., Shehadeh, J., Wellington, C.L., Leavitt, B.R., Baimbridge, K.G., Hayden, M.R. and Raymond, L.A. (2004) Potentiation of NMDA receptor-mediated excitotoxicity linked with intrinsic apoptotic pathway in YAC transgenic mouse model of Huntington's disease. *Mol. Cell. Neurosci.*, **25**, 469–479.

61. Slow, E.J., van Raamsdonk, J., Rogers, D., Coleman, S.H., Graham, R.K., Deng, Y., Oh, R., Bissada, N., Hossain, S.M., Yang, Y.-Z. *et al.* (2003) Selective striatal neuronal loss in a YAC128 mouse model of Huntington disease. *Hum. Mol. Genet.*, **12**, 1555–1567.

62. Van Raamsdonk, J.M., Pearson, J., Slow, E.J., Hossain, S.M., Leavitt, B.R. and Hayden, M.R. (2005) Cognitive dysfunction precedes neuropathology and motor abnormalities in the YAC128 mouse model of Huntington's disease. *J. Neurosci.*, **25**, 4169–4180.

63. Hsia, A.Y., Masliah, E., McConlogue, L., Yu, G.Q., Tatsuno, G., Hu, K., Kholodenko, D., Malenka, R.C., Nicoll, R.A. and Mucke, L. (1999) Plaque-independent disruption of neural circuits in Alzheimer's disease mouse models. *Proc. Natl Acad. Sci. USA*, **96**, 3228–3233.

64. Troy, C.M., Akpan, N. and Jean, Y.Y. (2011) Regulation of caspases in the nervous system implications for functions in health and disease. *Prog. Mol. Biol. Transl. Sci.*, **99**, 265–305.

65. LeBlanc, A., Liu, H., Goodyer, C., Bergeron, C. and Hammond, J. (1999) Caspase-6 role in apoptosis of human neurons, amyloidogenesis, and Alzheimer's disease. *J. Biol. Chem.*, **274**, 23426–23436.

66. Henshall, D.C., Skradski, S.L., Meller, R., Araki, T., Minami, M., Schindler, C.K., Lan, J.Q., Bonislawski, D.P. and Simon, R.P. (2002) Expression and differential processing of caspases 6 and 7 in relation to specific epileptiform EEG patterns following limbic seizures. *Neurobiol. Dis.*, **10**, 71–87.

67. Narkilahti, S. and Pitkänen, A. (2005) Caspase 6 expression in the rat hippocampus during epileptogenesis and epilepsy. *Neuroscience*, **131**, 887–897.

68. Nguyen, N., Lee, S.B., Lee, Y.S., Lee, Y.S., Lee, K.-H. and Ahn, J.-Y. (2009) Neuroprotection by NGF and BDNF against neurotoxin-exerted apoptotic death in neural stem cells are mediated through Trk receptors, activating PI3-kinase and MAPK pathways. *Neurochem. Res.*, **34**, 942–951.

69. Yu, L.-Y., Saarma, M. and Arumäe, U. (2008) Death receptors and caspases but not mitochondria are activated in the GDNF- or BDNF-deprived dopaminergic neurons. *J. Neurosci.*, **28**, 7467–7475.

70. Nguyen, T.L., Kim, C.K., Cho, J.H., Lee, K.H. and Ahn, J.Y. (2010) Neuroprotection signaling pathway of nerve growth factor and brain-derived neurotrophic factor against staurosporine induced apoptosis in hippocampal H19–7/IGF-IR [corrected]. *Exp. Mol. Med.*, **42**, 583–595.

71. Abidin, I., Eysel, U.T., Lessmann, V. and Mittmann, T. (2008) Impaired GABAergic inhibition in the visual cortex of brain-derived neurotrophic factor heterozygous knockout mice. *J. Physiol. (Lond.)*, **586**, 1885–1901.

72. Tanaka, J.-I., Horiike, Y., Matsuzaki, M., Miyazaki, T., Ellis-Davies, G.C.R. and Kasai, H. (2008) Protein synthesis and neurotrophin-dependent structural plasticity of single dendritic spines. *Science*, **319**, 1683–1687.

73. Poo, M.M. (2001) Neurotrophins as synaptic modulators. *Nat. Rev. Neurosci.*, **2**, 24–32.

74. Panagiotaki, N., Dajas-Bailador, F., Amaya, E., Papalopulu, N. and Dorey, K. (2010) Characterisation of a new regulator of BDNF signalling, Sprouty3, involved in axonal morphogenesis in vivo. *Development*, **137**, 4005–4015.

75. Gross, I., Armant, O., Benosman, S., de Aguilar, J.L., Freund, J.N., Kedinger, M., Licht, J.D., Gaiddon, C. and Loeffler, J.P. (2007) Sprouty2 inhibits BDNF-induced signaling and modulates neuronal differentiation and survival. *Cell Death Differ.*, **14**, 1802–1812.

76. Gorski, J.A., Zeiler, S.R., Tamowski, S. and Jones, K.R. (2003) Brain-derived neurotrophic factor is required for the maintenance of cortical dendrites. *J. Neurosci.*, **23**, 6856–6865.

77. Bekinschtein, P., Cammarota, M., Izquierdo, I. and Medina, J.H. (2008) BDNF and memory formation and storage. *Neuroscientist*, **14**, 147–156.

78. Bekinschtein, P., Cammarota, M., Katche, C., Slipczuk, L., Rossato, J.I., Goldin, A., Izquierdo, I. and Medina, J.H. (2008) BDNF is essential to promote persistence of long-term memory storage. *Proc. Natl Acad. Sci. USA*, **105**, 2711–2716.

79. Rauskolb, S., Zagrebelsky, M., Dreznjak, A., Deogracias, R., Matsumoto, T., Wiese, S., Erne, B., Sendtner, M., Schaeren-Wiemers, N., Korte, M. *et al.* (2010) Global deprivation of brain-derived neurotrophic factor in the CNS reveals an area-specific requirement for dendritic growth. *J. Neurosci.*, **30**, 1739–1749.

80. Ricobaraza, A., Cuadrado-Tejedor, M., Marco, S., Perez-Otano, I. and Garcia-Osta, A. (2010) Phenylbutyrate rescues dendritic spine loss associated with memory deficits in a mouse model of Alzheimer disease. *Hippocampus*. [Epub ahead of print].

81. Shirayama, Y., Chen, A.C.-H., Nakagawa, S., Russell, D.S. and Duman, R.S. (2002) Brain-derived neurotrophic factor produces antidepressant effects in behavioral models of depression. *J. Neurosci.*, **22**, 3251–3261.

82. Eisch, A.J., Bolaños, C.A., de Wit, J., Simonak, R.D., Pudiak, C.M., Barrot, M., Verhaagen, J. and Nestler, E.J. (2003) Brain-derived neurotrophic factor in the ventral midbrain-nucleus accumbens pathway: a role in depression. *Biol. Psychiatry*, **54**, 994–1005.

83. Berton, O., McClung, C.A., Dileone, R.J., Krishnan, V., Renthal, W., Russo, S.J., Graham, D., Tsankova, N.M., Bolanos, C.A., Rios, M. *et al.* (2006) Essential role of BDNF in the mesolimbic dopamine pathway in social defeat stress. *Science*, **311**, 864–868.

84. Bazzu, G., Calia, G., Puggioni, G., Spissu, Y., Rocchitta, G., Debetto, P., Grigoletto, J., Zusso, M., Migheli, R., Serra, P.A., Desole, M.S. and Miele, E. (2010) Alpha-synuclein-and MPTP-generated rodent models of Parkinsons disease and the study of extracellular striatal dopamine dynamics: a microdialysis approach. *CNS Neurol. Disord. Drug Targets*, **9**, 482–490.

85. Aggleton, J.P., Keen, S., Warburton, E.C. and Bussey, T.J. (1997) Extensive cytotoxic lesions involving both the rhinal cortices and area TE impair recognition but spare spatial alternation in the rat. *Brain Res. Bull.*, **43**, 279–287.

86. Liu, P. and Bilkey, D.K. (2001) The effect of excitotoxic lesions centered on the hippocampus or perirhinal cortex in object recognition and spatial memory tasks. *Behav. Neurosci.*, **115**, 94–111.

87. Brown, M.W. and Aggleton, J.P. (2001) Recognition memory: what are the roles of the perirhinal cortex and hippocampus? *Nat. Rev. Neurosci.*, **2**, 51–61.

88. Xiang, J.Z. and Brown, M.W. (1999) Differential neuronal responsiveness in primate perirhinal cortex and hippocampal formation during performance of a conditional visual discrimination task. *Eur. J. Neurosci.*, **11**, 3715–3724.

89. Guo, H., Pétrin, D., Zhang, Y., Bergeron, C., Goodyer, C.G. and LeBlanc, A.C. (2006) Caspase-1 activation of caspase-6 in human apoptotic neurons. *Cell Death Differ.*, **13**, 285–292.

90. Zhang, L., Xing, Y., Ye, C.F., Ai, H.X., Wei, H.F. and Li, L. (2006) Learning-memory deficit with aging in APP transgenic mice of Alzheimer's disease and intervention by using tetrahydroxystilbene glucoside. *Behav. Brain Res.*, **173**, 246–254.

91. Tohda, C., Naito, R. and Joyashiki, E. (2008) Kihi-to, a herbal traditional medicine, improves Abeta(25–35)-induced memory impairment and losses of neurites and synapses. *BMC Complement. Altern. Med.*, **8**, 49.

92. Velloso, N.A., Dalmolin, G.D., Gomes, G.M., Rubin, M.A., Canas, P.M., Cunha, R.A. and Mello, C.F. (2009) Spermine improves recognition memory deficit in a rodent model of Huntington's disease. *Neurobiol. Learn. Mem.*, **92**, 574–580.

93. Jiang, C.H., Tsien, J.Z., Schultz, P.G. and Hu, Y. (2001) The effects of aging on gene expression in the hypothalamus and cortex of mice. *Proc. Natl Acad. Sci. USA*, **98**, 1930–1934.

94. Wellington, C.L., Ellerby, L.M., Gutekunst, C.-A., Rogers, D., Warby, S., Graham, R.K., Loubser, O., van Raamsdonk, J., Singaraja, R., Yang, Y.-Z. *et al.* (2002) Caspase cleavage of mutant huntingtin precedes neurodegeneration in Huntington's disease. *J. Neurosci.*, **22**, 7862–7872.

95. Potts, P.R., Singh, S., Knezek, M., Thompson, C.B. and Deshmukh, M. (2003) Critical function of endogenous XIAP in regulating caspase activation during sympathetic neuronal apoptosis. *J. Cell Biol.*, **163**, 789–799.

96. Taylor, M.D., Holdeman, A.S., Weltmer, S.G., Ryals, J.M. and Wright, D.E. (2005) Modulation of muscle spindle innervation by neurotrophin-3 following nerve injury. *Exp. Neurol.*, **191**, 211–222.

97. Mayhew, T.M. and Olsen, D.R. (1991) Magnetic resonance imaging (MRI) and model-free estimates of brain volume determined using the Cavalieri principle. *J. Anat.*, **178**, 133–144.

98. Sonmez, O.F., Odaci, E., Bas, O., Colakoglu, S., Sahin, B., Bilgic, S. and Kaplan, S. (2010) A stereological study of MRI and the Cavalieri principle combined for diagnosis and monitoring of brain tumor volume. *J. Clin. Neurosci.*, **17**, 1499–1502.